

# Parametric source of two-photon states with a tunable degree of entanglement and mixing: Experimental preparation of Werner states and maximally entangled mixed states

C. Cinelli, G. Di Nepi, F. De Martini, M. Barbieri, and P. Mataloni

*Dipartimento di Fisica and Istituto Nazionale per la Fisica della Materia, Università di Roma "La Sapienza," Roma, 00185, Italy*

(Received 29 July 2003; revised manuscript received 1 April 2004; published 27 August 2004)

A parametric source of polarization-entangled photon pairs with striking spatial characteristics is reported. The distribution of the output electromagnetic  $\mathbf{k}$  modes excited by spontaneous parametric down-conversion and coupled to the output detectors can be very broad. Using these states realized over a full entanglement ring output distribution, the nonlocal properties of the generated entanglement have been tested by standard Bell measurements and by Ou-Mandel interferometry. A "mode-patchwork" technique based on the quantum superposition principle is adopted to synthesize in a straightforward and reliable way any kind of mixed state, of large conceptual and technological interest in modern quantum information. Tunable Werner states and maximally entangled mixed states have indeed been created by this technique and investigated by quantum tomography. A study of the entropic and nonlocal properties of these states has been undertaken experimentally and theoretically, by a unifying variational approach.

DOI: 10.1103/PhysRevA.70.022321

PACS number(s): 03.67.Mn, 03.65.Ta, 03.65.Ud, 03.65.Wj

## I. INTRODUCTION

Entanglement represents the irrevocable signature of quantum nonlocality. The striking key process was the Einstein-Podolsky-Rosen (EPR) discovery, followed by a much debated endeavor ended in the last few decades by Bell's inequalities and their experimental verification [1–3]. In recent years the violation of these inequalities has been tested so many times by optical experiments that (almost) no one today challenges the completeness of quantum theory.

In the modern science of quantum information (QI), entanglement represents the basic process underlying quantum computation [4], quantum teleportation [5,6], and some kinds of cryptographic communication schemes [7].

It appears highly significant that the most successful and reliable applications of entanglement have been obtained so far in the field of quantum optics. There the electromagnetic modes are associated with qubits which are generally encoded by the field polarization ( $\pi$ ) [8]. This type of qubit encoding is precisely the one considered in the present work. The  $\pi$  entanglement arises within the spontaneous emission process (spontaneous parametric down-conversion or SPDC) in a nonlinear (NL) optical crystal under suitable conditions, as we shall see shortly. In this process a pair of correlated photons are generated at wavelengths (WL's)  $\lambda_1$  and  $\lambda_2$  and momenta  $\hbar\mathbf{k}_1$  and  $\hbar\mathbf{k}_2$  by a quantum electrodynamical (QED) annihilation process of a pump photon with WL  $\lambda_p$  and momentum  $\mathbf{k}_p$ . Conservation of energy,  $\lambda_1^{-1} + \lambda_2^{-1} = \lambda_p^{-1}$ , and momentum, i.e., the phase-matching condition  $\mathbf{k}_1 + \mathbf{k}_2 = \mathbf{k}_p$ , leads to frequency and  $\mathbf{k}$ -vector correlation of the emitted photons. In the condition of entanglement the bipartite Hilbert space  $H_1 \otimes H_2$  with  $\dim(H_1) = \dim(H_2) = 2$  is spanned by the four-Bell-state entangled basis,

$$\begin{aligned} |\Psi^\pm\rangle &= 2^{-1/2}(|H_1, V_2\rangle \pm |V_1, H_2\rangle), \\ |\Phi^\pm\rangle &= 2^{-1/2}(|H_1, H_2\rangle \pm |V_1, V_2\rangle), \end{aligned} \quad (1)$$

where  $H$  and  $V$  correspond to the horizontal and vertical linear field's polarizations and the shorthand  $|X_1, Y_2\rangle \equiv |X\rangle_1$

$\otimes |Y\rangle_2$  will be used henceforth. The source of entanglement adopted today almost exclusively in quantum optics is based on SPDC in a type II noncollinear "phase-matched" NL crystal in which a pair of mutually orthogonally polarized photons is generated over a set of correlated directions corresponding to two different emission cones [9]. The cones intersect each other in two particular correlated modes with  $\mathbf{k}$  vectors  $\mathbf{k}_i$ ,  $i=1,2$ . The overall quantum state emitted over these two modes is generally expressed by either Bell state  $|\Psi^\pm\rangle$ , depending on the preset NL crystal orientation. By a careful spatial selection of the two correlated  $\mathbf{k}$  vectors  $\mathbf{k}_i$ , e.g., by two narrow pinholes, a high-purity entangled state may be generated by this kind of source. The typical achievable coincidence count rate is of the order of a few hundreds per second in a typical case involving a 1-mm-thick NL crystal excited by a 100 mW uv pump laser. Kwiat *et al.* realized a different source of  $\pi$ -entangled pairs, an order of magnitude brighter than the previous one, based on SPDC emission by a set of two thin, orthogonally oriented type I crystal slabs placed in mutual contact [10]. In that source the spatial indistinguishability of the two crystal emission cones, with orthogonal polarizations  $H$  and  $V$ , was responsible for the polarization entanglement.

In the present work we report on a SPDC source of polarization-entangled pairs, based on an interferometric scheme representing a folded version of Kwiat's source [10,11]. By this scheme it is possible to manipulate the superposition state by acting separately on one of the two emission cones and to detect, at least in principle, all SPDC entangled pairs emitted over the entire set of wave vectors excited by any parametric scattering process. In particular, we have investigated in the present work the most efficient, according to quantum optics,  $\lambda$ -degenerate process:  $\lambda_1 = \lambda_2 = 2\lambda_p$ . In fact, the parametric gain  $g$ , which is a function of the down-conversion frequencies, attains a maximum when  $\lambda_1 = \lambda_2$ ,  $g \propto \sqrt{(2\pi c)^2 / \lambda_1 \lambda_2 n_1(\lambda_1) n_2(\lambda_2)}$  [12]. Nonlocality tests performed with this source may have a particular significance regarding the conceptual difficulties related to the de-

tection loophole [13]. This loophole is properly ascribable to the limited efficiency of the detectors as well as to the loss of the correlated pairs created in any single QED spontaneous emission process that cannot reach the detectors for geometrical reasons. We shall discuss this subtle process in a forthcoming paper dealing with nonlocality tests undertaken with (Bell-Bohm) and without (Hardy) having recourse to inequalities [3,14,15].

The present work is mostly devoted to investigating theoretically and experimentally a quite different branch of QI, concerned with the properties of several relevant families of entangled mixed states. Because of the unavoidable effects of the decohering interactions these states are today indeed considered the basic constituents of modern QI and quantum computation, as they limit the performance of all quantum-communication protocols including quantum dense coding [16] and quantum teleportation [5,6]. It is not surprising that in the last few years, within an endeavor aimed at the use of mixed states as a practical resource, an entire branch of arduous mathematics and topology has been created to investigate the unexplored theory of the positive maps ( $P$  maps) in Hilbert spaces in view of the assessment of the “residual entanglement” and of the establishment of more general “state-separability” criteria [17–19].

A consistent and wide-ranging investigation of these useful and appealing aspects of modern physics requires the availability of a flexible source by which entangled pure as well as mixed states of any structure could be easily engineered in a reliable and reproducible way. The parametric-source described in the present work indeed possesses these properties and, consistently with the above considerations, it has been applied to the realization and a quantum tomographic analysis of Werner states [21–24] and maximally entangled mixed states (MEMS) [25,26].

The work is organized as follows. In Sec. II the source is fully described. Moreover, the high quality of the realized output entangled state is demonstrated by a Bell-inequality test showing the attainment of a nonlocal interferometric visibility as large as  $V \geq 0.94$  and a violation of a Bell inequality by 213 standard deviations. Section III reports on a “patchwork” method to generate a full set of Werner states. In addition, the results of a quantum tomographic investigation of their properties will be reported. In Sec. IV the methods of the previous section will be extended to a theoretical and experimental study of the MEMS. In Sec. V the EPR nonlocality of the MEMS and of the Werner states will be taken up in a unifying manner by a variational analysis of the correlation functions. Finally, the foreseeable perspectives of the presented method will be outlined in Sec. VI.

## II. THE PARAMETRIC SOURCE

The active element of our source of polarization-entangled photon pairs consisted of a single type-I NL thin crystal slab,  $\beta$ -barium borate (BBO), excited in two opposite directions ( $\mathbf{k}_p, -\mathbf{k}_p$ ) by a uv pump beam with WL  $\lambda_p$ , back-reflected by a spherical mirror ( $M$ ) (Fig. 1). Each of the two equal but independent SPDC processes generated pairs of correlated photons with wavelengths  $\lambda_i$  ( $i=1,2$ ), equal polar-

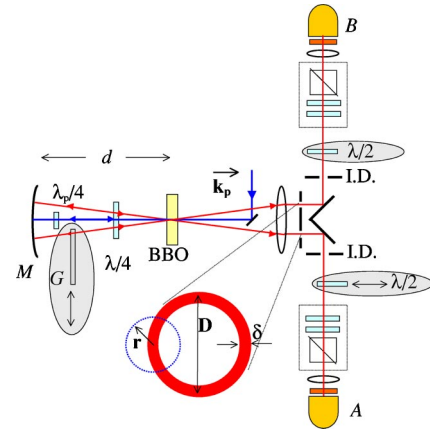


FIG. 1. Layout of the universal, high-brilliance source of polarization-entangled photon states and of general mixed states. Inset: Entanglement ring and pinhole of radius  $r$  for spatial selection.

izations ( $\pi$ ), and a spatial distribution of the corresponding, mutually correlated vectors  $\mathbf{k}_i$  consisting of two equal, opposite circular cones (dubbed here  $\mathbf{k}$  cones) with axes  $\mathbf{k}_p, -\mathbf{k}_p$  [9,10]. While all the relevant features of the present source are shared by all *non degenerate* phase-matched WL configurations, i.e.,  $\lambda_1^{-1} + \lambda_2^{-1} = \lambda_p^{-1}$  with  $\lambda_1 \neq \lambda_2$ , our present demonstration has been carried out for the degenerate case for simplicity and without loss of generality:  $\lambda_1 = \lambda_2 = \lambda = \lambda_p/2 = 727.6$  nm. Suppose that the NL crystal orientation is preset to generate SPDC pairs on both  $\mathbf{k}$  cones with any linear polarization, say  $\pi = H$ . Each pair of each  $\mathbf{k}$  cone is then emitted with a product state  $|H_1, H_2\rangle$  over its own four-dimensional Hilbert space. Suppose now that the two  $\mathbf{k}$  cones are made to overlap into a *single* one with axis  $\mathbf{k}_p$ , i.e., directed toward the right-hand side (RHS) of Fig. 1, by back-reflection over  $M$  of the  $\mathbf{k}$  cone with axis  $-\mathbf{k}_p$ . If in the flight from the crystal to  $M$  and back, in the “ $d$  section” in Fig. 1, the polarization of the corresponding emitted pairs is flipped, i.e.,  $H_i \rightarrow V_i$ , and a phase  $\phi$  is added, the state of the pair detected on the RHS of Fig. 1 is the entangled state

$$|\Phi\rangle = 2^{-1/2}(|H_1, H_2\rangle + e^{i\phi}|V_1, V_2\rangle). \quad (2)$$

Since this argument holds for any pair of correlated  $\mathbf{k}_i$  vectors emitted with equal probability and equal WL  $\lambda$ , all diametrically opposite points of the spatial circle obtained by interception of the output cone with a plane orthogonal to  $\mathbf{k}_p$ , i.e., belonging to the entanglement ring as we shall see shortly, are correlated by the same entanglement condition and thus represented by  $|\Phi\rangle$ . Of course, as for all quantum-interference phenomena, the  $\mathbf{k}$ -cone overlap should be perfect so as to realize the indistinguishability in principle of the actual origin of the detected pair for any set of ideal detectors coupled to the source output. All this represents the key process underlying the quantum behavior of the present device.

Let us now give more details about the apparatus (Fig. 1). A type I, 0.5-mm-thick, crystal was excited by a slightly focused  $V$ -polarized cw  $\text{Ar}^+$  laser beam ( $\lambda_p = 363.8$  nm) with wave vector  $-\mathbf{k}_p$ , i.e., directed toward the LHS in Fig. 1. The two correlated photons belonging to any SPDC couple had

common  $H$  polarization and were emitted with equal probability over a corresponding pair of wave vectors belonging to the surface of a circular cone with axis  $-\mathbf{k}_p$  and aperture  $\alpha \approx 2.9^\circ$ . The emitted radiation and the laser beam were then backreflected by the same spherical mirror  $M$  with curvature radius  $R=15$  cm, highly reflecting both  $\lambda$  and  $\lambda_p$ , placed at a distance  $d=R$  from the NL crystal. This value has been chosen in order to obtain a  $d$  section long enough to easily insert optical elements.

A zero-order  $\lambda/4$  wave plate (WP) placed between  $M$  and the NL crystal twice intercepted both backreflected  $\lambda$  and  $\lambda_p$  beams and then rotated by  $\pi/2$  the polarization of the backreflected field with WL  $\lambda$  while leaving virtually undisturbed the polarization state of the uv pump beam. In fact, it was verified that the  $\lambda/4$  WP acted very like a  $\lambda_p/2$  WP since  $\lambda_p=\lambda/2$ . For this purpose we measured the Stokes parameters of the pump beam, after a single transmission through the  $\lambda/4$  WP [22]. The experimental values of the Stokes parameters are

$$\text{Incident pump:}(1, -0.999, -0.00909, 0.0594),$$

$$\text{Transmitted pump:}(1, 0.913, -0.0500, -0.1550);$$

hence the pump polarization is almost completely rotated from  $V$  to  $H$ .

The phase  $\phi$  ( $0 \leq \phi \leq \pi$ ) of the generated pure entangled state, Eq. (2), was reliably controlled by micrometric displacements  $\Delta d$  of  $M$  along  $\mathbf{k}_p$ . The phase stability, representing the most challenging experimental problem, was solved by the use of the same back mirror  $M$  for both WL's  $\lambda$  and  $\lambda_p$  (see Appendix A). A positive lens ( $f=15$  cm) transformed the overall emission conical distribution into a cylindrical one with axis  $\mathbf{k}_p$ , whose transverse circular section identified the entanglement ring (ER) with diameter  $D=2\alpha F$ . Each couple of points symmetrically opposed through the center of the ring were then correlated by quantum entanglement, as we said. An annular mask with diameter  $D=1.5$  cm and width  $\delta=0.07$  cm provided in the present experiment a very accurate spatial selection of the ER. This one was divided into two equal portions along a vertical axis by a prismlike two-mirror system and then focused by two lenses on the active surfaces of two independent photodiodes  $\mathcal{A}$  and  $\mathcal{B}$  (Alice and Bob) by which standard Bell measurements could be performed by means of polarization analyzers ( $\vec{\pi}$ ). The detectors were silicon avalanche model SPCM-AQR14 with quantum efficiency (QE) of 65% and dark count rate  $\approx 50$  s $^{-1}$ . Typically, two equal interference filters, placed in front of  $\mathcal{A}$  and  $\mathcal{B}$  with bandwidth  $\Delta\lambda=6$  nm, determined the coherence time of the emitted photons:  $\tau_{\text{coh}} \approx 140$  fs. Optionally, the focusing could have been done on the ends of two polarization-preserving light pipes conveying the radiation to two far-apart detection stations  $\mathcal{A}$  and  $\mathcal{B}$ .

The insertion of one (or several) wave plates or filters partially (or fully) intercepting the radiation associated with the  $\mathbf{k}$  cones in (or outside) the  $d$  zone allowed the realization of various configurations of relevant physical significance. For instance, the insertion of a zero-order  $\lambda/2$  WP in one of the output detection arms allowed us to locally transform Eq. (2) into the state

$$|\Psi\rangle = 2^{-1/2}(|H_1, V_2\rangle + e^{i\phi}|V_1, H_2\rangle). \quad (3)$$

Then, by easily setting  $\phi=0$  or  $\phi=\pi$  the state expressed by Eq. (1) could be locally transformed into any one of the remaining three Bell states. Furthermore, and most important, the optional insertion of a zero-order  $\lambda_p/4$  WP in the  $d$  zone intercepting *only* the uv beam allowed the engineering of tunable nonmaximally entangled states. As shown by Hardy, using this class of states expressed as

$$|\Phi\rangle = \alpha|H_1, H_2\rangle + \beta|V_1, V_2\rangle, \alpha \neq \beta, |\alpha|^2 + |\beta|^2 = 1, \quad (4)$$

the nonlocality of quantum mechanics could be tested without recourse to inequalities (Hardy's ladder proof) [15]. In our system, the rotation of the uv WP by an angle  $\theta_p$  determined a  $\pi$  rotation of the backreflected uv pump beam with respect to the optical axes of the (fixed) NL crystal slab. The consequent  $\theta_p$ -tunable unbalancing of the SPDC efficiencies over the two  $\mathbf{k}$  cones affected the two interfering product-state terms in Eq. (2) by a coefficient proportional to  $\cos^2 2\theta_p$ . By adjusting  $\theta_p$  in the range  $0-\pi/4$ , the degree of entanglement  $\gamma=|\alpha/\beta|$  could be continuously tuned between 1 and 0 [27]. As emphasized later, preliminary results of the Hardy ladder proof obtained using the present source have been successfully reported in [11].

All these considerations are but a preliminary demonstration of the extreme flexibility of the present source. In the following sections we shall learn how, by a simple "patchwork" technique, pure states can be easily transformed into mixed states with various degrees of mixing. This allows us to undertake a comprehensive study of relevant classes of quantum states such as the Werner states and the maximally entangled mixed states.

#### A. Generation of postselected two-photon states

The quantum state of any photon pair generated by our source should be analyzed by accounting for the excited electromagnetic (e.m.) modes. Assume that each SPDC event is represented by the linear superposition of correlated pairs of e.m. modes, where each pair is represented by the set of  $\mathbf{k}$  vectors  $\{\mathbf{k}_1, \mathbf{k}_2\}$ . These modes are coupled within any elementary three-wave parametric scattering process whose excitation is allowed by phase matching. Because of the low parametric gain, as we shall see below, at most one pair can be generated. In this approximation, the overall entangled state expressing the detection of a single SPDC pair at the output of our source, after overlapping and activation of the  $\phi$  phase delay, is expressed by the quantum superposition

$$|\Phi\rangle = |0\rangle + C \int d^3k_1 d^3k_2 f(\mathbf{k}_1, \mathbf{k}_2) \times (a_{\mathbf{k}_1, H}^\dagger a_{\mathbf{k}_2, H}^\dagger + e^{i\phi} a_{\mathbf{k}_1, V}^\dagger a_{\mathbf{k}_2, V}^\dagger) |0\rangle, \quad (5)$$

where  $a_{\mathbf{k}_i, H}^\dagger$  ( $a_{\mathbf{k}_i, V}^\dagger$ ) is the creation operator of an  $H$ - ( $V$ -) polarized photon on the  $\mathbf{k}_i$  mode ( $i=1, 2$ ),  $f(\mathbf{k}_1, \mathbf{k}_2)$  is a proper function which accounts for nonperfect phase matching due to the finite dimensions of the NL crystal, and the integrals are taken over all the allowed modes.

In a typical SPDC-based quantum optics experiment, the set of  $\{\mathbf{k}_1, \mathbf{k}_2\}$  mode pairs coupled to the detectors is reduced

by the use of narrow spatial-filtering pinholes or single-mode optical fibers [6,8,9,28]. This operation allows us to select a pair of correlated  $\mathbf{k}$ -vectors, within a mode uncertainty  $\Delta\mathbf{k}$ . In these conditions, it may happen that only one photon in a pair passes through the spatial filter, while the other one is intercepted. A similar effect can be ascribed to any frequency-filtering operation as well. As a consequence, a state is obtained that is given by the superposition of the polarization-entangled pairs with single-photon states, in addition to the vacuum field. However, in the common case of a coincidence experiment, the output state may be considered as a postselected two-photon state. This postselection may cause conceptual difficulties when performing nonlocality tests [29].

With our source the adoption of postselection to eliminate the single-photon-state contribution would not be necessary in principle. Indeed, this would be possible by coupling the full set of mode pairs to detectors  $\mathcal{A}$  and  $\mathcal{B}$ , in all possible wavelength configurations, either degenerate ( $\lambda_1=\lambda_2$ ) or nondegenerate ( $\lambda_1\neq\lambda_2$ ). Of course, in this case severe limitations for full particle detection come from the limited  $\lambda$  extension of the detectors QE's and of the performance of the optical components (mirrors, lenses, etc.). Nevertheless, an ideal experiment may be conceived by which the full set of QED excited modes at any wavelength, ranging from a very large  $\lambda$  down to  $\lambda=\lambda_p$ , can be coupled to the detectors without any geometrical or frequency constraint, i.e., without any spatial or  $\lambda$  filtering. The same idealization is possible for the source of Kwiat *et al.* [10].

### B. Bell's inequalities test

The  $|\Phi^-\rangle$  Bell state has been adopted to test the violation of a Bell inequality by a standard coincidence technique and by the experimental configuration shown in Fig. 1 [30]. According to previous considerations, the distribution of active e.m. modes appearing in Eq. (5) and corresponding to the whole ER was spatially filtered by the annular mask.

The adopted angle orientations of the  $\vec{\pi}$ -analyzers located at the  $\mathcal{A}$  (1) and  $\mathcal{B}$  (2) sites were  $\{\theta_1=0, \theta'_1=45^\circ\}$  and  $\{\theta_2=22.5^\circ, \theta'_2=67.5^\circ\}$ , together with the corresponding orthogonal angles  $\{\theta_1^\perp, \theta'_1^\perp\}$  and  $\{\theta_2^\perp, \theta'_2^\perp\}$ . Using these values, the standard Bell inequality parameter can be evaluated [31]:

$$S = |P(\theta_1, \theta_2) - P(\theta_1, \theta'_2) + P(\theta'_1, \theta_2) + P(\theta'_1, \theta'_2)|, \quad (6)$$

where

$$P(\theta_1, \theta_2) = \frac{[C(\theta_1, \theta_2) + C(\theta_1^\perp, \theta_2^\perp) - C(\theta_1, \theta_2^\perp) - C(\theta_1^\perp, \theta_2)]}{[C(\theta_1, \theta_2) + C(\theta_1^\perp, \theta_2^\perp) + C(\theta_1, \theta_2^\perp) + C(\theta_1^\perp, \theta_2)]}$$

and  $C(\theta_1, \theta_2)$  is the coincidence rate measured at sites  $\mathcal{A}$  and  $\mathcal{B}$ . The measured value  $S=2.5564\pm 0.0026$  [11], obtained by integrating the data over 180 s, corresponds to a violation as large as 213 standard deviations with respect to the limit value  $S=2$  implied by local realistic theories [3,31,32]. As for the full set of measurements reported in the present paper, the good performance of the apparatus was largely attributable to the high brightness of the source, because of which large sets of statistical data could be accumulated in short

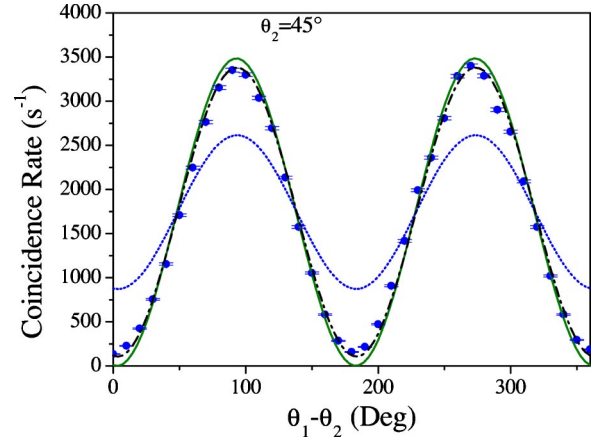


FIG. 2. Bell inequalities test. The selected state is  $|\Phi^-\rangle = (1/\sqrt{2})(|H_1, H_2\rangle - |V_1, V_2\rangle)$ .

measurement times with a low uv pump power.

The experimental data given in Fig. 2 show the  $\vec{\pi}$  correlation obtained by varying the angle  $\theta_1$  in the range  $45^\circ - 135^\circ$ , keeping the angle  $\theta_2=45^\circ$  fixed. The interference pattern shows the high degree of  $\pi$  entanglement of the source. The measured visibility of the coincidence rate,  $V\geq 94\%$ , gives a strong indication of the entangled nature of the state over the entire emission  $\mathbf{k}$  cone, while the single count rates do not show any periodic fringe behavior, as expected. In the same Fig. 2 the dotted line corresponds to the limit boundary between the quantum and the classical regimes [30], while the theoretical continuous curve expresses the ideal interferometric pattern with maximum visibility  $V=1$ .

The entanglement character of the source has also been investigated by a standard Ou-Mandel interferometric test [11,33], in this case by adoption of the Bell state expressed by Eq. (3) (Fig. 3, inset). For this experiment the radius of the iris diaphragms (ID) in Fig. 1 was set at  $r=0.075$  cm. The experimental results shown in Fig. 3 and corresponding to the values  $\phi=\pi$  and  $\phi=0$  express a value of the interference visibility  $V\approx 88\%$ . The full width at half maximum ( $\approx 35$   $\mu\text{m}$ ) of the interference pattern is in good agreement

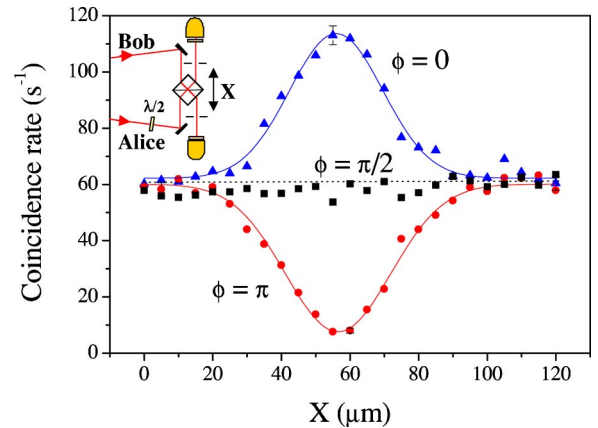


FIG. 3. Coincidence rate versus the position  $X$  of the beam splitter in the Ou-Mandel experiment. In the inset the corresponding interferometric apparatus is shown. The selected state is  $|\Psi\rangle = (1/\sqrt{2})(|H_1, V_2\rangle + e^{i\phi}|V_1, H_2\rangle)$ .

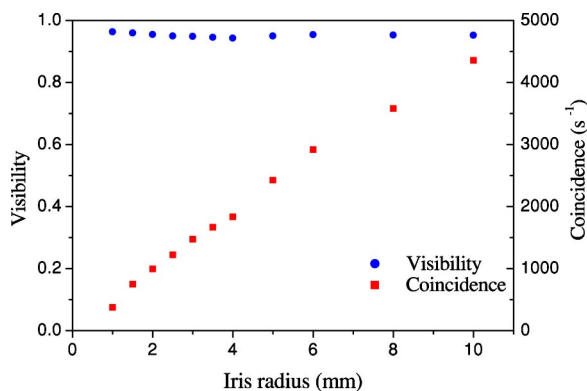


FIG. 4. Plot of the fringe visibility (circles, left axis) and coincidence rate (squares, right axis) as a function of the iris diaphragm radius  $r$ .

with the expected value evaluated for a filter bandwidth  $\Delta\lambda=6$  nm. In the same Fig. 3 the experimental results corresponding to the expected noninterference condition  $\phi = \pi/2$  are also shown for comparison.

We have characterized the robustness and the brightness of the source by measuring coincidences for different values of the radius  $r$  of the ID with a polarizing beam splitter placed in front of the detectors. This corresponds to select different portions of the ER, with area  $S=2D\delta \arcsin(r/D)$  (Fig. 1, inset). The experimental results of Fig. 4 demonstrate that a coincidence rate larger than  $4 \times 10^3 \text{ s}^{-1}$  at a pump power  $P \approx 100$  mW is measured over the entire ER when  $H_1, H_2$  or  $V_1, V_2$  pairs are selected and accidental coincidences are subtracted, while visibility maintains a value  $V \approx 0.94$ . Correspondently, a single-photon count rate of  $6 \times 10^4 \text{ s}^{-1}$  has been measured, with background counts subtracted. This corresponds to an overall measured efficiency of the apparatus  $\eta \approx 0.07$ . Hence, we can evaluate the generation rate of produced entangled pairs to exceed  $9 \times 10^3 \text{ s}^{-1} \text{ mW}^{-1}$  over the 6 nm filter bandwidth. A similar result has been reported with the two-crystal geometry source in Ref. [10]. On the other hand, because of the continuous-wave (cw) uv excitation regime, the NL parametric gain is so small,  $g < 10^{-3}$ , that the ratio of the probabilities of simultaneous SPDC generation of two photon pairs and of a single pair is  $\leq 10^{-6}$ . As a consequence, the emission of a double pair is taken to be negligible with cw pumping.

The present demonstration has been carried out in the  $\lambda$ -degenerate condition, i.e., implying the largest QED emission probability according to quantum optics. Note, however, that the favorable properties of the apparatus are not impaired by any general  $\lambda$ -nondegenerate dynamics. As said, among other properties this would allow, at least in principle and by the use of sufficiently broadband detectors, the lossless detection of the (almost) complete set of SPDC-generated photon pairs.

### III. GENERATION AND TOMOGRAPHIC CHARACTERIZATION OF WERNER STATES

Because of the peculiar spatial superposition property of the output state shown by the structure of Eq. (5), the present

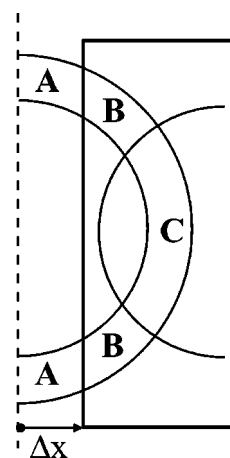


FIG. 5. Partition of the (half) ER for Werner state production.

apparatus appears to be an ideal source of any bipartite, two-qubit entangled state, either pure or mixed, in particular of the Werner state [21]

$$\rho_W = p|\Psi^-\rangle\langle\Psi^-| + \frac{1-p}{4}\mathbf{I}_4 \quad (7)$$

consisting of a mixture of a pure singlet state  $|\Psi^-\rangle = 2^{-1/2}\{|HV\rangle - |VH\rangle\}$  with probability  $p$  ( $0 \leq p \leq 1$ ) and a fully mixed state expressed by the unit operator  $\mathbf{I}_4$  defined in the four-dimensional Hilbert space. The corresponding density matrix, expressed in the basis  $|HH\rangle, |HV\rangle, |VH\rangle, |VV\rangle$ , is

$$\rho_W = \begin{pmatrix} A & 0 & 0 & 0 \\ 0 & B & C & 0 \\ 0 & C & B & 0 \\ 0 & 0 & 0 & D \end{pmatrix} \quad (8)$$

with  $A=D=\frac{1}{4}(1-p)$ ,  $B=\frac{1}{4}(1+p)$ ,  $C=-p/2$ . The Werner states possess high conceptual and historical value because, in the probability range  $[1/3 < p < 1/\sqrt{2}]$ , they do not violate any Bell's inequality in spite of being entangled states, i.e., negative partial transpose (NPT) states [18,20].

Among many possible alternatives, we synthesized these states by means of a convenient ‘‘patchwork’’ technique based again on the quantum-superposition principle. This procedure requires only the three optical elements shown in the gray regions of Fig. 1. They were arranged in the experimental layout according to the following steps.

(1) Making reference to the original source state expressed by Eq. (2), a singlet state  $|\Psi^-\rangle$  was easily obtained by inserting a  $\pi$ -flipping, zero-order  $\lambda/2$  WP in front of detector  $\mathcal{B}$ .

(2) An antireflection-coated glass plate  $G$ , 200  $\mu\text{m}$  thick, inserted in the  $d$  section with a variable transverse position  $\Delta x$ , introduced a decohering fixed time delay  $\Delta t > \tau_{coh}$  that spoiled the in-principle indistinguishability of the intercepted portions of the overlapping quantum-interfering radiation  $\mathbf{k}$  cones, represented by the B+C sectors of the ER in Fig. 5. This ‘‘distinguishability issue’’ is easily understood by thinking that the induced  $\Delta t$  delay in principle allows an ideal

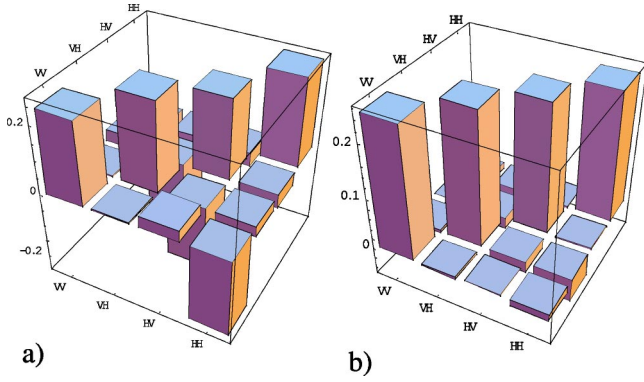


FIG. 6. Tomographic reconstruction (real parts) of the mixture  $(1/2)[|\Phi^-\rangle\langle\Phi^-| + |\Psi^-\rangle\langle\Psi^-|]$  with linear entropy  $S_L = 0.696 \pm 0.017$  and tangle  $T = 0.0154 \pm 0.0046$  (a) and  $\mathbf{I}_4/4$  (b) ( $S_L = 0.9874 \pm 0.0036$ ,  $T = 0 \pm 0.011$ ).

detector, i.e., one with infinite time resolution, to identify the  $\mathbf{k}$  cones from which the detected photon came.

As a consequence, in the intercepted sector B+C, the statistical mixture  $\frac{1}{2}[|H_1, V_2\rangle\langle H_1, V_2| + |V_1, H_2\rangle\langle V_1, H_2|]$  was generated, while the nonintercepted sector A expressed the polarization pure-state singlet contribution to  $\rho_W$ . In other words, all nondiagonal elements of  $\rho_W$  corresponding to the surface sectors B+C of the ER, the ones optically intercepted by  $G$ , were set to zero.

(3) A  $\lambda/2$  WP was inserted in the semicylindrical photon distribution reflected by the beam-splitting prism toward the detector  $\mathcal{A}$ . Its position was carefully adjusted in order to intercept half of the B+C sector, i.e., by making  $B=C$  (Fig. 5). Note that only half of the ER needed to be intercepted by the optical plates, by virtue of the EPR nonlocality. In summary, the sector A of the ER contributed to  $\rho_W$  with a pure state  $p|\Psi^-\rangle\langle\Psi^-|$ , the sector B+C=2B with the statistical mixture  $[(1-p)/4]\{|H_1, V_2\rangle\langle H_1, V_2| + |V_1, H_2\rangle\langle V_1, H_2| + |H_1, H_2\rangle\langle H_1, H_2| + |V_1, V_2\rangle\langle V_1, V_2|\}$  and the probability  $p$ , a monotonic function of  $\Delta x$  ( $p \propto \Delta x$  for small  $p$ ), could be easily varied over its full range of values, from  $p=0$  ( $\rho_W = \frac{1}{4}\mathbf{I}_4$ ) to  $p=1$  ( $\rho_W = |\Psi^-\rangle\langle\Psi^-|$ ) [34]. Optionally, the setting of the  $\lambda/2$  wp intercepting the beam towards  $\mathcal{A}$  could be automatically activated by the single setting  $\Delta x$  via an electromechanical servo.

As an example, we may give here a demonstration of the feasibility of our technique by synthesizing the identity matrix  $\mathbf{I}/4$  (Fig. 6). First insert the  $\lambda/2$  WP in channel  $\mathcal{A}$  to intercept  $\frac{1}{4}$  of the ER: in this way the mixture  $\frac{1}{2}[|\Phi^-\rangle\langle\Phi^-| + |\Psi^-\rangle\langle\Psi^-|]$  is produced [Fig. 6(a)]. Then, the complete era-

sure of nondiagonal elements of the matrix is performed by making a  $\Delta t$ -delay glass plate  $G$  to intercept half of the ER [Fig. 6(b)].

Any Werner state could be realized by a similar patchwork technique, by setting  $B=C$  and by adjusting the value of  $p(\Delta x)$ . Far more generally, all possible bipartite states in  $2 \times 2$  dimensions could be created by this technique, as we shall see shortly. This indeed expresses the flexibility of our source.

The tomographic reconstructions of three different Werner states, with weights  $p = 0.82$  (a),  $p = 0.47$  (b), and  $p = 0.27$  (c), are shown in Fig. 7 [22].

As anticipated at the beginning of the present section, the Werner states have been introduced as examples of nonseparable states that, in a limited range of  $p$ , do not violate the Clauser-Horne-Shimony-Holt (CHSH) inequality. These states are also important for quantum information, since they model a decoherence process occurring on a singlet state traveling along a noisy channel [23].

We may investigate these processes in a more detailed fashion on the basis of some relevant entropic properties of the mixed states. A relevant property of any mixed state, the *tangle*  $T = [C(\rho)]^2$ , i.e., the square of the concurrence  $C(\rho)$ , is directly related to the *entanglement of formation*  $E_F(\rho)$  and expresses the degree of entanglement of  $\rho$  [35]. Another important property of the mixed states is the *linear entropy*  $S_L = d(1 - \text{Tr } \rho^2)/(d-1)$ ,  $S_L = (1-p^2)$  for the Werner states, which quantifies the degree of disorder, viz., the mixedness of a system with dimension  $d$  [36]. By virtue of the very definition of  $C(\rho)$ , these two quantities are found to be related, for the Werner states, as follows:

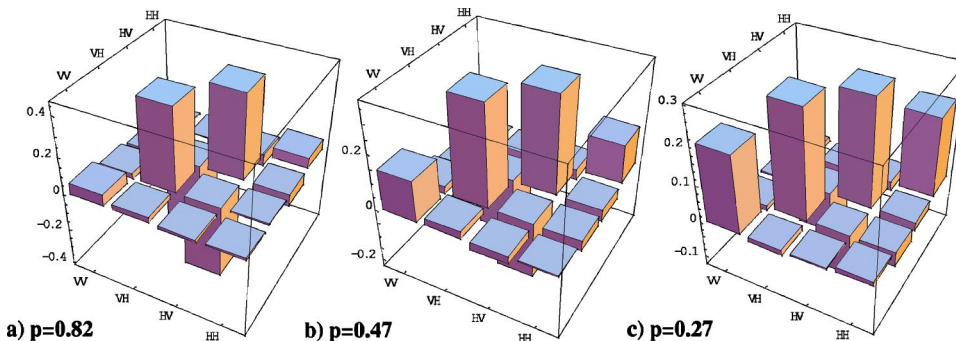


FIG. 7. Tomographic reconstruction of three different Werner states with different singlet weights  $p$  and fidelity  $F = 0.919 \pm 0.019$ ,  $F = 0.950 \pm 0.013$ , and  $F = 0.978 \pm 0.019$ , respectively. The imaginary components are negligible.

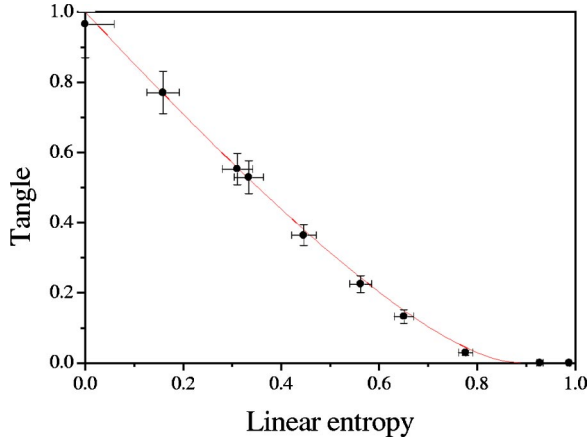


FIG. 8. Tangle vs linear entropy for experimentally generated Werner states. Continuous line corresponds to the theoretical curve.

$$T_W(S_L) = \begin{cases} \frac{1}{4}(1 - 3\sqrt{1 - S_L})^2 & \text{for } 0 \leq S_L \leq \frac{8}{9}, \\ 0 & \text{for } \frac{8}{9} \leq S_L \leq 1. \end{cases} \quad (9)$$

Since if and only if the state is separable is  $T=0$ , we deduce that the Werner states are not separable in the range  $0 \leq S_L < 8/9$  or, equivalently, in the range  $1/3 < p \leq 1$ . Several Werner states have been experimentally synthesized by the present technique and the corresponding experimental values are plotted in the  $T$  vs  $S_L$  plane (Fig. 8) [24]. The agreement between experimental data and reported theoretical plot appears to be good. For the states shown in Fig. 7, we have obtained  $(S_L, T) = (0.334 \pm 0.029, 0.529 \pm 0.047)$  (a),  $(S_L, T) = (0.776 \pm 0.014, 0.0290 \pm 0.0069)$  (b), and  $(S_L, T) = (0.9278 \pm 0.0066, 0 \pm 0.0019)$  (c).

We performed a tomographic analysis of the entangled state used for the measurements described in Sec. II B and obtained the following values for tangle and linear entropy:  $T = 0.987 \pm 0.096$ ,  $S_L = 0 \pm 0.059$ . The corresponding point is shown in Fig. 8.

We have recently adopted the Werner states generated by the present technique to perform the first experimental realization of the entanglement witness, a powerful method conceived to detect entanglement with few local measurements [37].

#### IV. GENERATION AND TOMOGRAPHIC CHARACTERIZATION OF MEMS

As a final demonstration of the flexibility of our method, a set of maximally entangled mixed states has been synthesized by our source and tested again by quantum tomography [22,25,38]. On the other hand, according to the introductory notes expressed above, the MEMS are to be considered, for practical reasons, as peculiar ingredients of modern quantum information because their entanglement cannot be increased by any unitary transformation. Since this property holds also for the Werner states, these can be assumed to belong to the broader class of MEMS. A formal proof of this statement is found in Appendix B [39].

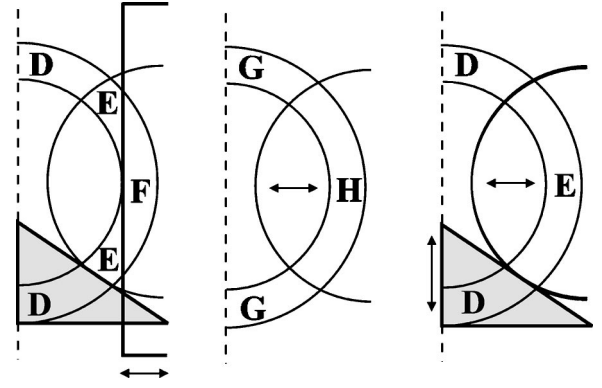


FIG. 9. Partition of the (half) ER for MEMS production: (a) left  $\mathbf{k}$  cone for  $0 \leq p \leq 2/3$ , (b) right  $\mathbf{k}$  cone, and (c) left  $\mathbf{k}$  cone for  $2/3 \leq p \leq 1$ .

The MEMS generated and tested by our method are expected, by definition, to own the maximum tangle  $T$  allowed by a given value of linear entropy  $S_L$ . The density matrix  $\rho_{MEMS}$  is again represented by the matrix given by Eq. (8) with the parameters  $A \equiv 1 - 2g(p)$ ,  $B \equiv g(p)$ ,  $C \equiv -\frac{1}{2}p$ ,  $D \equiv 0$ . There,  $g(p) = \frac{1}{2}p$  for  $p \geq 2/3$  and  $g(p) = 1/3$  for  $p < 2/3$ . The expression for  $T$ , obtained by a procedure similar to the one adopted for the Werner states, is

$$T_{MEMS}(S_L) = \begin{cases} \frac{1}{4} \left( 1 + \sqrt{1 - \frac{3}{2}S_L} \right)^2 & \text{for } 0 \leq S_L \leq \frac{16}{27}, \\ \frac{4}{3} - \frac{3}{2}S_L & \text{for } \frac{16}{27} \leq S_L \leq \frac{8}{9}. \end{cases} \quad (10)$$

Two different partition techniques for the ER have been adopted to generate the MEMS, depending on the value of the singlet weight, either  $p < 2/3$  or  $p \geq 2/3$ . Let us consider three different experimental steps for  $p < 2/3$ .

(1) The  $\lambda/2$  WP was inserted in the semicylindrical photon distribution reflected by the beam-splitting prism toward the detector  $\mathcal{A}$  in order to partition in equal sectors the two rings corresponding to the left  $\mathbf{k}$  cone [ $D = E + F$ ; Fig. 9(a)] and to the right  $\mathbf{k}$  cone [ $G = H$ ; Fig. 9(b)]. This generated at the output the statistical mixture  $|V_1, V_2\rangle\langle V_1, V_2|$ ,  $|V_1, H_2\rangle\langle V_1, H_2|$ ,  $|H_1, H_2\rangle\langle H_1, H_2|$ ,  $|H_1, V_2\rangle\langle H_1, V_2|$ .

(2) Sector D of the left  $\mathbf{k}$  cone, corresponding to  $|V_1, V_2\rangle\langle V_1, V_2|$ , was erased by inserting a right-angle opaque screen [Fig. 9(a)], while sector G of the right  $\mathbf{k}$  cone, corresponding to  $|H_1, H_2\rangle\langle H_1, H_2|$  was kept unaltered [Fig. 9(b)].

(3) The glass plate  $G$  was inserted in the  $d$  section of the source in order to intercept a portion  $1 - p$  of the sector E of the left  $\mathbf{k}$  cone, F in Fig. 9(a). As for the generation of the Werner states, this procedure spoiled the indistinguishability of the intercepted portions of the overlapping radiation cones. The three identical nonzero diagonal terms corresponding to sector G and to the sectors overlapped with H, E, and F were  $|H_1, H_2\rangle\langle H_1, H_2|$ ,  $|V_1, H_2\rangle\langle V_1, H_2|$ ,  $|H_1, V_2\rangle\langle H_1, V_2|$ , for  $p$  varying in the range  $0 \leq p < 2/3$  by transverse displacement of  $G$ . In this way the ratio between the ER contributions E and F in the left  $\mathbf{k}$  cone could be continuously tuned.

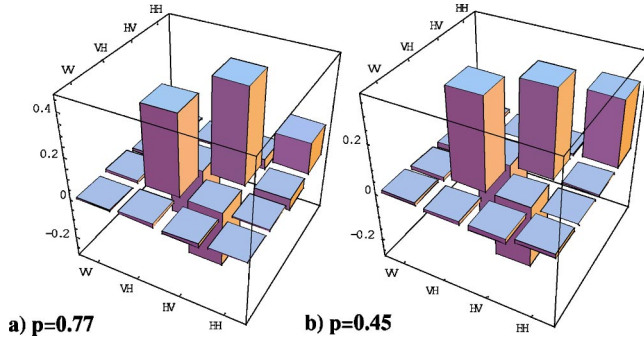


FIG. 10. Tomographic reconstruction (real parts) of two different MEMS. Corresponding singlet weights  $p$  are also shown. The fidelity values are  $F=0.972\pm 0.019$  and  $F=0.9635\pm 0.0085$ , respectively.

The larger the  $F$  contribution, the larger was the decoherence of the MEMS.

In the case  $p \geq 2/3$ , no retarding glass plate was needed to realize the MEMS. By fine adjustment of the  $\lambda/2$  WP the weight  $p$  of the singlet could be tuned in the range  $2/3 \leq p < 1$  and for each value of  $p$  the vertical position of the screen needed to be adjusted in order to erase the contribution  $|V_1, V_2\rangle\langle V_1, V_2|$  of sector D in Fig. 9(c).

Accurate experimental production of the MEMS was found to be particularly severe, likely because of the generally critical requirements needed for operating on the very boundary between the allowed and forbidden regions of the  $(S_L, T)$  plane [24]. In this sense any experimental loss of entanglement correlation within the singlet limited the quality of MEMS. For instance, the optical axis of the NL BBO crystal of our source was oriented in a vertical plane and a strong decoherence effect could arise from the spatial walkoff occurring in the crystal between the vertically polarized twin photons belonging to the left  $\mathbf{k}$  cone. This one was associated with the extraordinary index of refraction  $n_e(\zeta)$  of the crystal, where  $\zeta$  is the angle between the  $\mathbf{k}$  WV of each photon and the axis direction. This effect, which is also present in the  $\lambda/4$  WP, may be reduced by working with a small aperture angle  $\alpha$  of the emission cone. By varying the BBO axis orientation the MEMS were produced by reducing the cone aperture to the value  $\alpha \approx 1.4^\circ$ .

The tomographic results shown in Fig. 10 reproduce graphically and with fair accuracy two  $\rho_{MEMS}$  structures with parameters  $p=0.77$  (a) and  $p=0.45$  (b), corresponding to  $(S_L, T)=(0.356\pm 0.029, 0.603\pm 0.042)$  (a) and  $(S_L, T)=(0.702\pm 0.018, 0.195\pm 0.028)$  (b). Figure 11 shows the experimental behavior of several experimental MEMS in the  $(S_L, T)$  plane compared with the theoretical curves of Eqs. (9) and (14). The states produced lie close to the theoretical curve for MEMS; however, the agreement between the experimental results and the theoretical predictions was found to be far less satisfactory than for Werner states.

## V. NONLOCAL PROPERTIES OF MEMS

It is possible to investigate the nonlocal properties of MEMS by a general formalism, i.e., by following the quan-

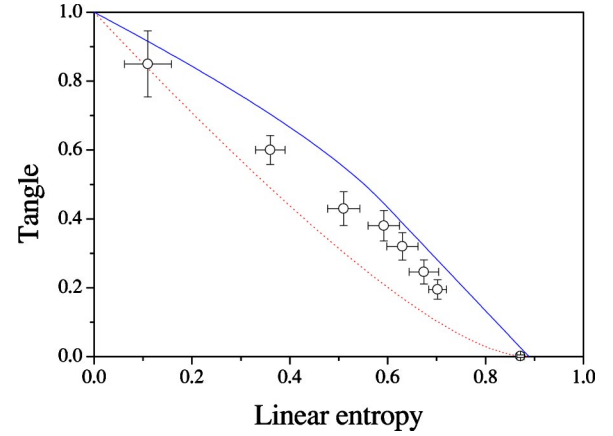


FIG. 11. Tangle vs linear entropy for experimentally generated MEMS. The continuous line represents the theoretical behavior; the dotted line is the expected curve for Werner states.

titative test adopted by Bell to investigate the completeness of quantum mechanics [3]. For two correlated spin- $\frac{1}{2}$  particles, with spin vectors  $\vec{s}_1$  and  $\vec{s}_2$ , the following inequality holds:

$$-2 \leq S = P(\hat{u}_1; \hat{u}_2) - P(\hat{u}_1; \hat{u}'_2) + P(\hat{u}'_1; \hat{u}_2) + P(\hat{u}'_1; \hat{u}'_2) \leq 2, \quad (11)$$

where  $\hat{u}_1$  and  $\hat{u}_2$  are unitary norm vectors related to the angular coordinates  $(\Theta_1, \Phi_1)$  and  $(\Theta_2, \Phi_2)$  in the Bloch sphere and  $P(\hat{u}_1; \hat{u}_2)$  is the correlation function,

$$P(\hat{u}_1; \hat{u}_2) = \langle (\hat{u}_1 \cdot \vec{s}_1)(\hat{u}_2 \cdot \vec{s}_2) \rangle. \quad (12)$$

Note that the angle  $\Theta$  on the Bloch sphere corresponds to the polarization angle  $\theta = \Theta/2$ . In the density matrix formalism the last expression can be written as

$$P(\hat{u}_1; \hat{u}_2) = \text{Tr}(\rho O_{12}), \quad (13)$$

where

$$O_{12} = O_1 \otimes O_2, \quad O_k = \begin{pmatrix} \cos \Theta_k & e^{-i\Phi_k} \sin \Theta_k \\ e^{i\Phi_k} \sin \Theta_k & -\cos \Theta_k \end{pmatrix}, \quad k = 1, 2.$$

By choosing  $\Theta_1=0$ ,  $\Theta_2=\pi/4$ ,  $\Theta'_1=\pi/2$ ,  $\Theta'_2=3\pi/4$ , and  $\Phi_1=\Phi_2=\Phi'_1=\Phi'_2=0$  one is led to the well known result  $S = 2\sqrt{2} > 2$  for a spin singlet  $|\Psi^-\rangle$ . In the case of the MEMS the general form of density matrix  $\rho$  given by Eq. (8) can be adopted with  $A, B, C = -\frac{1}{2}p$ , and  $D$  real numbers.  $D$  depends on the normalization condition:  $D = 1 - A - 2B$ . The correlation function becomes

$$P(\hat{u}_1; \hat{u}_2) = (1 - 4B) \cos \Theta_1 \cos \Theta_2 - p \cos(\Phi_1 - \Phi_2) \sin \Theta_1 \sin \Theta_2, \quad (14)$$

where the first term depends on the structure of the state via the diagonal term  $B$  while the second term is a function of the only singlet weight  $p$  in the mixture. This leads to the following general expression of the Bell parameter:

$$\begin{aligned}
S = & (1 - 4B)[\cos \Theta_1 \cos \Theta_2 - \cos \Theta_1 \cos \Theta'_2 + \cos \Theta'_1 \cos \Theta_2 \\
& + \cos \Theta'_1 \cos \Theta'_2] - p[\cos(\Phi_1 - \Phi_2) \sin \Theta_1 \sin \Theta_2 \\
& - \cos(\Phi_1 - \Phi'_2) \sin \Theta_1 \sin \Theta'_2 \\
& + \cos(\Phi'_1 - \Phi_2) \sin \Theta'_1 \sin \Theta_2 \\
& + \cos(\Phi'_1 - \Phi'_2) \sin \Theta'_1 \sin \Theta'_2]. \quad (15)
\end{aligned}$$

The inequality violation conditions are found by looking for an extremal point of  $S$ . It can be verified that  $\partial S / \partial \Theta_k = 0$  for  $\cos \Theta_1 = \cos \Theta_2 = \cos \Theta'_1 = \cos \Theta'_2 = 0$ . Let us set  $\Theta_1 = \Theta'_2 = -\pi/2$ ,  $\Theta'_1 = \Theta_2 = \pi/2$  as a convenient choice, and, by substitution, the expression

$$\begin{aligned}
S = & -p[\cos(\Phi_1 - \Phi_2) - \cos(\Phi_1 - \Phi'_2) + \cos(\Phi'_1 - \Phi_2) \\
& + \cos(\Phi'_1 - \Phi'_2)]
\end{aligned}$$

attains its minimum value  $S = -2\sqrt{2}p$  for  $\Phi_1 = -\Phi'_1 = \pi/4$ ,  $\Phi_2 = \pi/2$ ,  $\Phi'_2 = 0$ . Hence we find that the violation of the Bell inequalities is verified only for states with  $p > 1/\sqrt{2}$ , for any values of the diagonal terms  $A, B, D$ .

This result holds also for the Werner states, where  $A = D = \frac{1}{4}(1-p)$  and  $B = \frac{1}{4}(1+p)$ , as noted in Sec. III.

By a more elegant procedure, we could note that for any traceless operator  $O_{12}$  the expectation value in a state with weight  $p$  is given by

$$P(\hat{u}_1; \hat{u}_2) = \text{Tr}(\rho_W O_{12}) = pP_s(\hat{u}_1; \hat{u}_2). \quad (16)$$

The expression for the Bell inequality then becomes

$$-\frac{2}{p} \leq P_s(\hat{u}_1; \hat{u}_2) - P_s(\hat{u}_1; \hat{u}'_2) + P_s(\hat{u}'_1; \hat{u}_2) + P_s(\hat{u}'_1; \hat{u}'_2) \leq \frac{2}{p}, \quad (17)$$

which is violated for  $p > 1/\sqrt{2}$ , i.e.,  $S_L < 1/2$ . The corresponding experimental test requires the same angular setting of the  $\pi$  analyzer as for any standard Bell test performed for a pure singlet state and reported in Sec. II B.

Note that in the range  $p \in [1/\sqrt{2}, 1/3]$ , or equivalently in the range  $S_L \in [1/2, 8/9]$ , the Werner states, although not separable, do not violate the CHSH inequality [40].

In summary, for any Werner state  $\rho_W$  three regions can be distinguished: for  $1/\sqrt{2} < p \leq 1$  ( $0 \leq S_L < 1/2$ ),  $\rho_W$  is not separable and violates the CHSH inequality; for  $1/3 < p \leq 1/\sqrt{2}$  ( $1/2 \leq S_L < 8/9$ ),  $\rho_W$  is not separable and does not violate the CHSH inequality; and for  $0 \leq p \leq 1/3$  ( $8/9 \leq S_L \leq 1$ ),  $\rho_W$  is separable and does not violate the CHSH inequality.

The corresponding following values of the  $|S|$  parameter have been obtained experimentally for the states shown in Figs. 7(a)–7(c):  $|S| = 2.0790 \pm 0.0042$  [Fig. 7(a)],  $|S| = 1.049 \pm 0.011$  [Fig. 7(b)], and  $|S| = 0.4895 \pm 0.0047$  [Fig. 7(c)].

The test of Bell-CHSH inequalities has been performed for several experimentally synthesized Werner states. The relative behavior of  $|S|$  as a function of the weight  $p$  is shown in Fig. 12. The experimental data, placed under the theoretical straight line, show the effect of a nonperfect correlation within the singlet region A in Fig. 5.

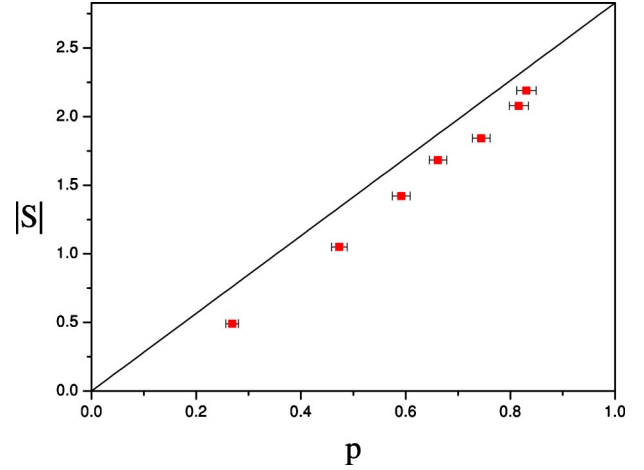


FIG. 12. Plot of the Bell parameter  $|S|$  as a function of weight  $p$ . The expected straight line  $|S| = 2\sqrt{2}p$  is also reported.

We may extend the above theoretical analysis to any MEMS state  $\rho_{MEMS}$  where  $A = 1 - 2g(p)$  and  $B = g(p)$ ,  $D = 0$ . The correlation function becomes

$$\begin{aligned}
P(\hat{u}_1; \hat{u}_2) = & [1 - 4g(p)] \cos \Theta_1 \cos \Theta_2 \\
& - p \cos(\Phi_1 - \Phi_2) \sin \Theta_1 \sin \Theta_2. \quad (18)
\end{aligned}$$

In this case the critical condition  $p = 1/\sqrt{2}$  occurs for the point with coordinates  $(S_L, T) = (0.552, 0.5)$ . An experimental test of Bell's inequality, performed with these states, involves observables with a complex phase term  $\Phi$ .

Two distinct regions can then be distinguished in the case of MEMS: for  $1/\sqrt{2} < p \leq 1$  ( $0 \leq S_L < 0.552$ ),  $\rho_{MEMS}$  is not separable and violates the CHSH inequality; for  $0 \leq p < 1/\sqrt{2}$  ( $0.552 \leq S_L < 8/9$ ),  $\rho_{MEMS}$  is not separable and does not violate the CHSH inequality.

## VI. CONCLUSION

The structural characteristics of the SPDC source of  $\pi$ -entangled photon pairs presented here and the way the quantum superposition principle underlying its performance is exploited are expected to suggest in the future an increasing number of sophisticated applications in the domain of quantum information and quantum communication and in the broader field dealing with the fundamental tests of quantum mechanics. We can think, for instance, of entanglement multiplexing in quantum-cryptographic networks, of schemes of joint entanglement over  $\vec{\pi}$  and  $\mathbf{k}$ -vector degrees of freedom, etc. As already mentioned, adding a spherical cavity to the device will allow the realization of a different kind of optical parametric oscillator synchronously pumped by a high-peak-power, mode-locked femtosecond uv source. This device would generate a multiphoton nonthermal entangled state over a spatially extended ER distribution of  $\mathbf{k}$  vectors. This idea is presently being investigated in our laboratory.

As far as applications to quantum-mechanical foundations are concerned, we already emphasized that the present device appears to be a suitable source of bipartite mixed states and of bipartite nonmaximally entangled states. In this last

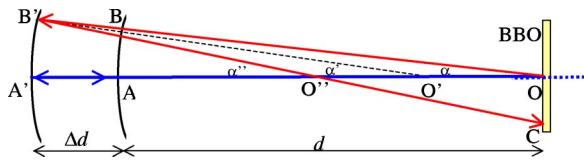


FIG. 13. Scheme representing the optical path difference within the single-arm interferometer.

respect, a comprehensive study of the verification of Hardy's ladder proof, a relevant and intriguing quantum nonlocality test, has been successfully completed recently [11] and will be reported extensively elsewhere. In our experiment the performance of the source allowed the attainment of the ladder's rung  $K=20$ , while previous experiments were necessarily limited to  $K \leq 3$  [15,17].

#### ACKNOWLEDGMENTS

Thanks are due to W. Von Klitzing and G. Giorgi for early involvement in the experiment and for useful discussions. This work was supported by the FET European Network on Quantum Information and Communication (Contract No. IST-2000-29681, ATESIT) and by PRA-INFM (CLON).

#### APPENDIX A: PHASE CONTROL OF THE ENTANGLED STATE

Because of its peculiar single-arm interferometer configuration, the high-brilliance source overcomes many of the instability problems due to the typical phase fluctuations of a standard two-arm interferometer. The spherical mirror  $M$  determines a large value of the displacement,  $|\Delta d| \approx 60 \mu\text{m}$  in our case, which allows the phase transition  $\phi=0 \rightarrow \phi=\pi$  from the Bell state  $|\Phi_+\rangle$  to the other  $|\Phi_-\rangle$ . This can be demonstrated by referring to Fig. 13. Starting from the condition  $d=R$  and neglecting for simplicity the BBO and  $\lambda/4$  WP thickness, a displacement  $\Delta d = OO' = AA' \neq 0$  determines different optical paths of the uv beam,  $2(OA')$ , and of the photon pair generated toward the left in Fig. 12 and reflected by mirror  $M$ ,  $2(OB' + B'C)$ . The factor of 2 which appears in the second optical path accounts for the two-photon emission over two symmetric directions with respect to  $\mathbf{k}_p$ . The

phase difference has the following expression:

$$\begin{aligned} \phi &= 4\pi(\overline{OA'})\lambda_p^{-1} - 4\pi(\overline{OB'} + \overline{B'C})\lambda^{-1} \\ &= 4\pi\lambda^{-1}[2(\overline{OA'}) - (\overline{OB'} + \overline{B'C})]. \end{aligned}$$

$\phi$  is function of the distances  $\overline{OA'}$ ,  $\overline{OB'}$ , and  $\overline{B'C}$ . Since  $\overline{OA} = \overline{OB} = \overline{O'A'} = \overline{O'B'} = R$ , we have  $\overline{OA'} = R + \Delta d$ . By approximating  $\alpha'' \cong \alpha' \cong \alpha$  and applying the Carnot theorem to the triangle  $OO'B'$ , we find the following expression:  $\overline{OB'} = \sqrt{(\Delta d)^2 + R^2 + 2R\Delta d \cos(\alpha)}$ . Finally the following equality holds:  $\overline{B'C} = \overline{O''C} + \overline{O''B'}$ , and it can be easily found that  $(\overline{O''B'}) = -(\overline{OO''})\cos(\alpha) + (\overline{OB'})$ , while  $\overline{O''C}$  is obtained by simple calculations.

Using the above results we easily find that the transition  $|\Phi_+\rangle \rightarrow |\Phi_-\rangle$  is obtained by a displacement  $|\Delta d| = 60 \mu\text{m}$ , which is in good agreement with the experimental results. Note that the condition  $\Delta d \neq 0$  implies a lateral displacement  $\overline{OC}$  of the reflected SPDC beams. Because of the intrinsic cylindrical symmetry,  $\overline{OC}$  may be viewed as the radius of an annular region which grows with  $\Delta d$  on the BBO plane. This geometrical effect makes the two emission cones distinguishable. It introduces a *spatial* decoherence which becomes relevant when  $\overline{OC}$  becomes comparable with the diameter of the *active* pumped region of the crystal ( $\approx 150 \mu\text{m}$ ). In our experimental conditions  $\overline{OC} \approx 10^{-1}\Delta d$ , we have observed that any coherent superposition of the state vanishes for  $|\Delta d| \gtrsim 600 \mu\text{m}$ .

#### APPENDIX B: WERNER STATES AS MEMS

By expressing the density matrix of a Werner state  $\rho_W$  in terms of the *fidelity*  $F$  representing the overlapping between any Werner state and  $|\Psi^-\rangle\langle\Psi^-|$ ,  $\rho_W = [(1-F)/3]\mathbf{I}_4 + [(4F-1)/3]|\Psi^-\rangle\langle\Psi^-|$ . Hence the expression for  $T$  is given by  $T(\rho_W) = (\max\{0, 2F-1\})^2$ . The condition for an entangled state implies that  $\frac{1}{2} < F \leq 1$  and  $T(\rho_W) = (2F-1)^2$ . A nonlocal unitary transformation  $U$  such that  $U|\Psi^-\rangle = |\Psi\rangle = \sqrt{a}|H_1, H_2\rangle + \sqrt{1-a}|V_1, V_2\rangle$ , expressed in terms of the parameter  $a \in [\frac{1}{2}, 1]$ , transforms  $\rho_W$  into the mixture  $\rho'_W = U\rho_W U^\dagger = [(1-F)/3]\mathbf{I}_4 + [(4F-1)/3]|\Psi\rangle\langle\Psi|$ . It has been demonstrated that  $\rho'_W$  is still entangled for  $\frac{1}{2} \leq a < \frac{1}{2}[1 + \sqrt{3(4F^2-1)}/4F-1]$  [39].  $T(\rho_W)$  is then maximized for  $a = \frac{1}{2}$ . As a consequence, any Werner state belongs to the class of MEMS.

- [1] E. Schrödinger, Proc. Cambridge Philos. Soc. **31**, 555 (1935).
- [2] L. Rosenfeld, in *Quantum Theory and Measurement*, edited by J. A. Wheeler and W. H. Zurek (Princeton University Press, Princeton, NJ, 1983).
- [3] J. S. Bell, *Speakable and Unsayable in Quantum Mechanics* (Cambridge University Press, Cambridge, England, 1988); A. Aspect, P. Grangier, and G. Roger, Phys. Rev. Lett. **49**, 91 (1982); M. Jammer, *The Philosophy of Quantum Mechanics* (Wiley, New York, 1974).
- [4] A. Ekert and R. Jozsa, Rev. Mod. Phys. **68**, 733 (1996); E. Knill, R. Laflamme, and G. J. Milburn, Nature (London)

**40946** (2001).

- [5] C. H. Bennett, G. Brassard, C. Crepeau, R. Jozsa, A. Peres, and W. K. Wootters, Phys. Rev. Lett. **70**, 1895 (1993).
- [6] D. Boschi, S. Branca, F. De Martini, L. Hardy, and S. Popescu, Phys. Rev. Lett. **80**, 1121 (1998); D. Bouwmeester *et al.*, Nature (London) **390**, 575 (1997); I. Marcikic *et al.*, *ibid.* **421**, 509 (2003).
- [7] A. Ekert, Nature (London) **358**, 14 (1992); N. Gisin *et al.*, Rev. Mod. Phys. **74**, 145 (2002).
- [8] E. Lombardi, F. Sciarrino, S. Popescu, and F. De Martini, Phys. Rev. Lett. **88**, 070402 (2002); S. Giacomini, F. Sciarrino

- rino, E. Lombardi, and F. De Martini, Phys. Rev. A **66**, 030302 (2002).
- [9] D. Klyshko, *Photons and Nonlinear Optics* (Gordon and Breach, New York, 1988); P. G. Kwiat *et al.*, Phys. Rev. Lett. **75**, 4337 (1995).
- [10] P. G. Kwiat, E. Waks, A. G. White, I. Appelbaum, and P. H. Eberhard, Phys. Rev. A **60**, R773 (1999).
- [11] G. Giorgi, G. Di Nepi, P. Mataloni, and F. De Martini, Laser Phys. **13**, 350 (2003); M. Barbieri, F. De Martini, G. Di Nepi, and P. Mataloni, e-print quant-ph/0303018.
- [12] A. Yariv, *Quantum Electronics*, 3rd ed. (Wiley, New York, 1988).
- [13] E. S. Fry, T. Walther, and S. Li, Phys. Rev. A **52**, 4381 (1995).
- [14] D. Bohm, *Quantum Mechanics* (Dover, New York, 1989), Chap. 23.
- [15] L. Hardy, Phys. Rev. Lett. **71**, 1665 (1993); D. Boschi, S. Branca, F. De Martini, and L. Hardy, *ibid.* **79**, 2755 (1997); G. Di Giuseppe, F. De Martini, and D. Boschi, Phys. Rev. A **56**, 176 (1997); Erkenntnis **45**, 367 (1997).
- [16] C. H. Bennett and S. J. Wiesner, Phys. Rev. Lett. **69**, 2881 (1992).
- [17] K. Kraus, *States, Effects and Operations: Fundamental Notions of Quantum Theory* (Wiley, New York, 1991).
- [18] A. Peres, Phys. Rev. Lett. **77**, 1413 (1996); L. Duan, G. Giedke, J. I. Cirac, and P. Zoller, *ibid.* **84**, 2722 (2000); R. Simon, *ibid.* **84**, 2726 (2000).
- [19] M. Lewenstein, D. Bruss, J. I. Cirac, B. Kraus, M. Kus, J. Samsonowicz, A. Sampera, and R. Tarrach, J. Mod. Opt. **47**, 2841 (2000); D. Bruss, J. I. Cirac, P. Horodecki, F. Hulpke, B. Kraus, and M. Lewenstein, *ibid.* **49**, 1399 (2002).
- [20] M. Horodecki, P. Horodecki, and R. Horodecki, Phys. Rev. Lett. **80**, 5239 (1998); *Quantum Information: An Introduction to Basic Theoretical Concepts and Experiments* (Springer, Berlin, 2001).
- [21] R. F. Werner, Phys. Rev. A **40**, 4277 (1989).
- [22] D. F. V. James, P. G. Kwiat, W. J. Munro, and A. G. White, Phys. Rev. A **64**, 052312 (2001).
- [23] M. A. Nielsen and I. L. Chuang, *Quantum Computation and Quantum Information* (Cambridge University Press, Cambridge, England, 2000).
- [24] A. G. White, D. F. V. James, W. J. Munro, and P. G. Kwiat, Phys. Rev. A **65**, 012301 (2001).
- [25] S. Ishizaka and T. Hiroshima, Phys. Rev. A **62**, 022310 (2000); W. J. Munro, D. F. V. James, A. G. White, and P. G. Kwiat, *ibid.* **64**, 030302 (2001); F. Verstraete, K. Audenaert, and B. De Moor, *ibid.* **64**, 012316 (2001).
- [26] M. Barbieri, F. De Martini, G. Di Nepi, and P. Mataloni, Phys. Rev. Lett. **92**, 177901 (2004).
- [27] For an alternative realization of nonmaximally entangled states, see A. G. White, D. F. V. James, P. H. Eberhard, and P. G. Kwiat, Phys. Rev. Lett. **83**, 3103 (1999).
- [28] C. Kurtsiefer, M. Oberparleiter, and H. Weinfurter, Phys. Rev. A **64**, 023802 (2001).
- [29] E. Santos, Phys. Rev. A **212**, 10 (1996); L. De Caro and A. Garuccio, Phys. Rev. A **50**, R2803 (1994).
- [30] Y. H. Shih and C. O. Alley, Phys. Rev. Lett. **61**, 2921 (1988); Z. Y. Ou and L. Mandel, *ibid.* **61**, 50 (1988).
- [31] J. F. Clauser, M. A. Horne, A. Shimony, and R. A. Holt, Phys. Rev. Lett. **23**, 880 (1969).
- [32] E. Santos, Phys. Rev. Lett. **66**, 1388 (1991); N. D. Mermin, *New Techniques and Ideas in Quantum Measurement* (New York Academy of Sciences, New York, 1986); A. Garuccio, Phys. Rev. A **52**, 2535 (1995).
- [33] C. K. Hong, S. Y. Ou, and L. Mandel, Phys. Rev. Lett. **59**, 2044 (1987).
- [34] For an alternative realization of the Werner state, see Y. S. Zhang, Y. F. Huang, C. F. Li, and G. C. Guo, Phys. Rev. A **66**, 062315 (2002).
- [35] W. K. Wootters, Phys. Rev. Lett. **80**, 2245 (1998); S. Bose and V. Vedral, Phys. Rev. A **61**, 040101 (2000); V. Coffman, J. Kundu, and W. K. Wootters, *ibid.* **61**, 052306 (2000). Since  $E_F(\rho)$ ,  $C(\rho)$ , and  $T$  are monotonic functions of one another, they are equivalent measures of entanglement.
- [36] T. C. Wei, K. Nemoto, P. M. Goldbart, P. G. Kwiat, W. J. Munro, and F. Verstraete, Phys. Rev. A **67**, 022110 (2003).
- [37] M. Barbieri, F. De Martini, G. Di Nepi, P. Mataloni, G. M. D'Ariano, and C. Macchiavello, Phys. Rev. Lett. **91**, 227901 (2003); O. Gühne, P. Hyllus, D. Bruß, A. Ekert, M. Lewenstein, C. Macchiavello, and A. Sanpera, Phys. Rev. A **66**, 062305 (2002).
- [38] P. Kwiat, J. Altepeter, D. Branning, E. Jeffrey, N. Peters, and T. C. Wey, e-print quant-ph/0303040; N. A. Peters, J. B. Altepeter, D. A. Branning, E. R. Jeffrey, T-C. Wei, and P. G. Kwiat, Phys. Rev. Lett. **92**, 133601 (2004).
- [39] T. Hiroshima and S. Ishizaka, Phys. Rev. A **62**, 044302 (2000).
- [40] J. Barrett, Phys. Rev. A **64**, 042305 (2001).